Pergamon

Solid State Communications, Vol. 103, No. 11, pp. 603–606, 1997

0038–1098/97 $17.00+.00

PII: S0038-1098(97)00276-7

COLLECTIVE EXCITATIONS IN GRAPHITE LAYERS

C.S. Huang,[a] M.F. Lin[a,b] and D.S. Chuu[a]

[a]Electrophysics Department, National Chiao Tung University, Hsinchu 30050, Taiwan, Republic of China
[b]Physics Department, National Cheng Kung University, Tainan 70101, Taiwan, Republic of China

(*Received* 8 *May* 1997; *accepted* 16 *June* 1997 *by A. Okiji*)

The π-electronic excitations in graphite layers are studied within the self-consistent-field approach. The π plasmon behaves as an optical plasmon, mainly due to the π-band characteristics. The excitation spectra and the π-plasmon frequencies are obviously enhanced by the interlayer Coulomb interactions and increase with the number of graphite layers. © 1997 Published by Elsevier Science Ltd.

Keywords: D. dielectric response, D. electron–electron interactions.

Carbon atoms can form diamond, graphite, carbon nanotube, C_{60}-related fullerene and carbon onion. Their physical properties might be similar to one another. For example, the π plasmon, the π-electronic collective excitations, exist in all systems except diamond, namely, graphite [1, 2], carbon nanotube [3], C_{60}-related fullerene [4] and carbon onion [5]. The layered graphite has been studied for many years. In this work, we mainly study the π plasmon in graphite layers. Its dependence on magnitude (q) and direction (ϕ) of the transferred momentum and interlayer Coulomb interactions is investigated.

The π and σ bands in graphite are formed, respectively, by $2p_z$ and ($2s$, $2p_x$, $2p_y$) orbitals. The excitation energy of the π band is below 15 eV, while the opposite is true for the σ band [1, 2]. The tight-binding model [6] is used to calculate the π band and the self-consistent-field approach (SCF) [7] to study the π-electronic excitations. The excitation properties will be strongly affected by the π-band characteristics. The π plasmon with frequency $w_p > 5$ eV is identified from the most prominent peak in electron-energy-loss spectrum (EELS). The graphite layers are weakly coupled to neighboring layers by Van der Waals interactions. Such interactions might modify the π band in the vicinity of the Fermi level [8]. However, they only affect the low-frequency physical properties, e.g. the intraband plasmon ~0.1 eV [9], but not the π plasmon. Thus, these interactions are neglected in the calculations. On the other hand, the interlayer Coulomb interactions among electrons on different layers play an important role in the π plasmon.

A graphite sheet is a hexagonal-symmetry plane. Each unit cell has two carbon atoms, so the Bloch functions could be described by the two tight-binding functions [$U_1(k_x, k_y)$ and $U_2(k_x, k_y)$] built from the $2p_z$ orbitals [6]. Diagonalizing the Hamiltonian with only the nearest-neighboring interactions, one can obtain the energy dispersions as:

$$E^{c,v}(k_x, k_y) = \pm \gamma_0 \left\{ 1 + 4\cos\left(\frac{3bk_y}{2}\right)\cos\left(\frac{\sqrt{3}bk_x}{2}\right) + 4\cos^2\left(\frac{\sqrt{3}bk_x}{2}\right)\right\}^{1/2}, \tag{1a}$$

and the Bloch functions are [6]

$$\Psi^{c,v}(k_x, k_y) = \frac{1}{\sqrt{2}}\left\{ U_1(k_x, k_y) \pm \frac{H_{12}^*(k_x, k_y)}{|H_{12}(k_x, k_y)|} U_2(k_x, k_y)\right\}. \tag{1b}$$

$$H_{12}(k_x, k_y) = -\gamma_0 \left\{ e^{-ik_y b} + 2e^{ibk_y/2}\cos\left(\frac{\sqrt{3}bk_x}{2}\right)\right\}$$

is the Hamiltonian matrix element. The resonance integral γ_0~2.3–2.7 eV [10] and $\gamma_0 = 2.5$ eV is taken in the calculations, $b = 1.42$ Å is the C–C bond length. The wave vectors, k_x and k_y, are confined within the first Brillouin zone [BZ; Fig. 1(a)]. The superscript $c(v)$ represents the conduction (valence) band. The conduction band is symmetric, about $E_F = 0$, to the valence

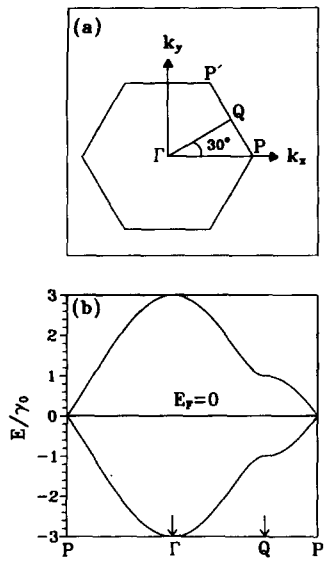

Fig. 1. (a) The first Brillouin zone of a graphite layer. The Γ point is the origin. The P and P' points are the corners and the Q point is the middle point between them. (b) The 2D π band.

band [Fig. 1(b)]. A single graphite layer is a zero-gap semiconductor.

The π band is anisotropic at the plane. Therefore, the electronic excitations are described by magnitude (q) and direction (ϕ) of the transferred momentum and excitation energy (w). $0° \leq \phi \leq 30°$ is sufficient to characterize the direction-dependent excitations owing to the hexagonal symmetry. For a single graphite layer, the dielectric function calculated from SCF [7] is

$$\epsilon(q,\phi,w) = \epsilon_0 - V_q\chi(q,\phi,w), \tag{2a}$$

where

$$\chi(q,\phi,w) = \int_{1\text{st}BZ} \frac{dk_x\,dk_y}{\pi^2} \times |\langle k_x+q_x, k_y+q_y; c|e^{iq_x x}\, e^{iq_y y}|k_x,k_y;v\rangle|^2 \times \frac{E^c(k_x+q_x,k_y+q_y)-E^v(k_x,k_y)}{E^c(k_x+q_x,k_y+q_y)-E^v(k_x,k_y)-(w+i\Gamma)}, \tag{2b}$$

$V_q = 2\pi e^2/q$ and $\epsilon_0 = 2.4$ is the background dielectric constant [1]. Γ is the energy width due to various deexcitation mechanisms. For a finite Γ, χ has to be modified according to Mermin [11]. The intraband excitations are clearly absent and the interband excitations are the only excitation channel.

There exist interlayer Coulomb interactions in the multilayered graphite. When an N-layer system is perturbed by a probing electron with the time-dependent potential $V^{ex}(q,\phi,w)$, the effective potential $V^{eff}(q,\phi,w)$ is the sum of the external potential and the induced potential from screening charges on all layers. Within the linear response [7], V_l^{eff} on the lth layer is given by

$$\epsilon_0 V_l^{eff}(q,\phi,w) = V_l^{ex}(q,\phi,w) + \sum_{l'} V_{l,l'}(q) V_{l'}^{eff}(q,\phi,w)\chi(q,\phi,w). \tag{3}$$

$V_l^{eff}\chi$ is the induced charge density on the l'th layer. The interlayer Coulomb interaction is $V_{l,l'}(q) = V_q \exp(-q|l-l'|I_c)$, where $I_c = 3.35$ Å is the periodic distance. V_l^{eff} could be obtained from the known external potential by solving the $N \times N$ matrix. Here the density distribution of the probing electron is assumed to be uniform inside the system. Such an approximation does not change the main features in the π-electronic excitations. It is reasonable for the smaller N, since the periodic distance is short. The probability, which the probing electron transfers (q, ϕ, w) to the N-layer system, is calculated from the Fermi *Golden Rule*

$$\sum_{l=1}^{N} -\text{Im}\,\chi|V_l^{eff}|^2 \equiv \left\langle \sum_{l=1}^{N} V_l^{ex} \right\rangle \text{Im}\left(\frac{-1}{\epsilon}\right). \tag{4}$$

$\langle\sum_{l=1}^{N} V_l^{ex}\rangle$ is the average external potential. $\text{Im}(-1/\epsilon)$ defined in equation (4) could be interpreted as the EELS intensity. When $N = \infty$, $\epsilon = \epsilon_0 - V_q \sinh(qI_c)\chi/(\cosh(qI_c)-1)$. This is the dielectric function of the $k_z = 0$ mode for the superlattice of the infinite graphite layers [12]. The π-electronic collective oscillations on all layers are indicated to be in phase.

The dielectric function of a single graphite layer [equation (2)] is calculated at $q = 0.25$ Å^{-1}, $\phi = 0°$ and $\Gamma = 0.1$ eV. The real part ϵ_1 is shown by the solid curve and the imaginary part ϵ_2 by the dashed curve (Fig. 2). The excitations due to the critical points in the energy-wave-vector space would cause singular

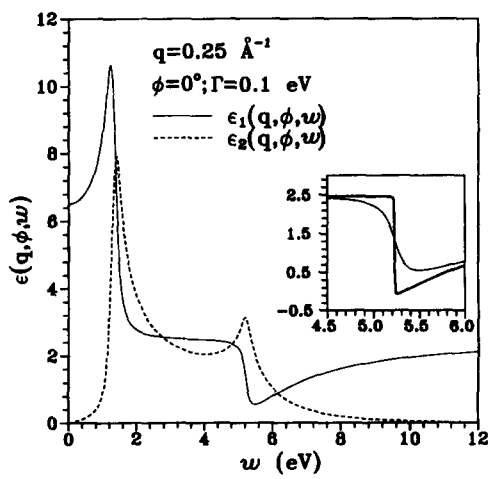

Fig. 2. The real (ϵ_1) and the imaginary (ϵ_2) parts of the dielectric function at $q = 0.25$ Å^{-1}, $\phi = 0°$ and $\Gamma = 0.1$ eV. ϵ_1 at $\Gamma \to 0$ (the heavy solid curve) is also shown in the inset for comparison.

structures in ϵ. They include the minimum [P; Fig. 1(a)], the maximum (P') and the saddle point (near Q). Note that the Q point is the saddle point only at $q = 0$. The excitation energy of the P point is the threshold energy. ϵ_2 (ϵ_1), which corresponds to P' and Q points, respectively, exhibits the square-root divergency (the square-root divergency) and the logarithmical divergency [13] (the diplike structure after broadening). When Γ approaches zero, the diplike structure in ϵ_1 would become the discontinuity which accompanies zeros of ϵ_1 (the heavy solid curve in the inset). The number of the singular structures might change with ϕ. For example, there are two logarithmic divergencies at $w \sim 5.5$ eV for $\phi = 30°$, since there are two saddle points near the middle points of the corners [Fig. 1(a)]. The main features remain similar as q changes. For $q = 0$, the diplike structure in ϵ_1 occurs at $w \sim 2\gamma_0$. Such a structure would become deep and occur at higher w in the increasing of q. It generally includes zeros of ϵ_1. The vanishing ϵ_1, if at where ϵ_2 is small, is associated with the π plasmon. That is, when the Landau damping is weak, EELS will exhibit a prominent plasmon peak.

The EELS, $\mathrm{Im}[-1/\epsilon(q, \phi, w)]$, is further shown in Fig. 3. The spectrum exhibits a weak and broad shoulder at low w's and a very pronounced peak at ~6 eV. The former is due to the e–h excitations. The latter remains strong even at very large Γ, e.g. $\Gamma = 0.5$ eV. It is thus reasonable to identify the most prominent peak as the π-electronic collective excitations. The π plasmon is closely related to the diplike structure in ϵ_1. This band-induced plasmon hardly exists in a graphite layer when q is very small, e.g. EELS at $q = 0.01$ Å^{-1} (the dashed curve in the inset). Also note that the π plasmon at $q \to 0$ could exist in graphite with $N = \infty$ (Fig. 4), mainly

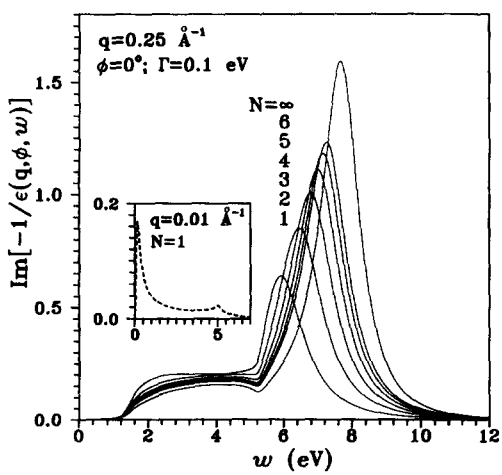

Fig. 3. The EELS for various graphite layers are calculated at $q = 0.25$ Å^{-1}, $\phi = 0°$ and $\Gamma = 0.1$ eV. The EELS of a single graphite layer at $q = 0.01$ Å^{-1} is also shown in the inset for comparison.

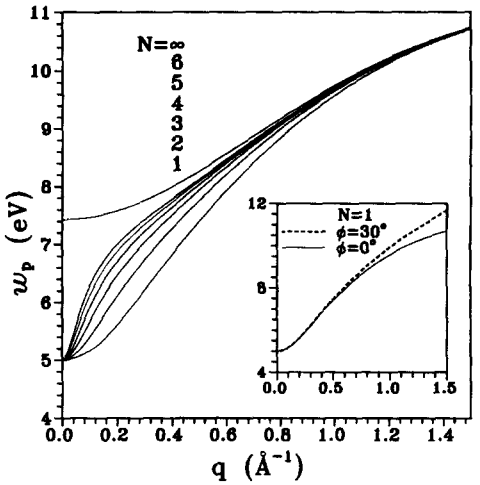

Fig. 4. The q-dependent plasmon frequencies for various graphite layers at $\phi = 0°$. The inset also shows $w_p(q)$ of a graphite layer at $\phi = 30°$.

due to the very strong interlayer Coulomb interactions. When the number of the graphite layers increases, the EELS intensity and the plasmon frequency behave similarly. The main reason for this is the interlayer Coulomb coupling.

The variation of plasmon frequency with q is shown in Fig. 4. The strong q-dependence directly reflects the π-band characteristic, the strong wave-vector-dependence. When N is finite, w_p approaches a finite value $2\gamma_0$ at $q \to 0$. This result further illustrates that the π plasmon is associated with the interband excitations of the saddle points. The π plasmon apparently belongs to an optical plasmon. The interlayer Coulomb interactions obviously enhance the plasmon frequency at small q's. Moreover, for graphite at $q \to 0$, they cause the blue-shift of the plasmon frequency from 5 eV to 7.4 eV. This value is close to the measured result (~7 eV) of the reflectance spectrum [1] and the EELS [2]. Finally, the q-dependent plasmons also rely on ϕ. The excitation energies of the saddle points strongly depend on ϕ only at large q's and so does the ϕ-dependence of w_p (inset).

The π-band characteristics, the strong wave-vector-dependence, the anisotropic behaviour and the special symmetry, are directly reflected in the excitation properties. The critical points in the energy-wave-vector space could induce the singular structures in the dielectric functions and thus are associated with the π-electronic collective excitations. The π plasmon behaves like an optical plasmon. The interlayer Coulomb interactions play an important role in enhancing the EELS intensity and the plasmon frequencies. The dependence of the π plasmon on the number of graphite layers needs further experimental verification.

Acknowledgements—This work was supported in part by the National Science Council of Taiwan, Republic of China under the Grant No. 86-2112-M-009-006.

REFERENCES

1. Taft, E.A. and Philipp, H.R., *Phys. Rev.*, **138,** 1965, A197.
2. Zeppenfeld, K., *Z. Phys.*, **243,** 1971, 229.
3. Kuzuo, R., *et al., Jpn. J. App. Phys.*, **31,** 1992, L1484; Draid, V.P., *et al., Science*, **259,** 1993; 1601; Ajayan, P.M., *et al., Phys. Rev.*, **B47,** 1993, 6859; Bursill, L.A., *et al., Phys. Rev.*, **B49,** 1994, 2882.
4. Gensterblum, G. *et al., Phys. Rev. Lett.*, **67,** 1991, 2171.
5. Lucas, A.A. *et al., Phys. Rev.*, **B49,** 1994, 2888.
6. Wallace, P.R., *Phys. Rev.*, **71,** 1947, 622.
7. Ehrenreich, H. *et al., Phys. Rev.*, **115,** 1959, 786.
8. Charlier, J.-C. *et al., Phys. Rev.*, **B44,** 1992, 13237.
9. Jesen, E.T. *et al., Phys. Rev. Lett.*, **66,** 1991, 492.
10. Sloczewski, J.C., *et al., Phys. Rev.*, **109,** 1958, 272; Tsukada, M.T., *et al., J. Phys. Soc. Jpn.*, **32,** 1972, 54; Blinowski, J., *et al., J. Phys. (Paris)*, **41,** 1980, 47; Charlier, J.-C., *et al., Phys. Rev.*, **B46,** 1992, 4531; McClure, J.W., *et al., Phys. Rev.*, **B104,** 1956, 666.
11. Mermin, N.D., *Phys. Rev.*, **B1,** 1970, 2362.
12. Shung, K.W.-K., *Phys. Rev.*, **B34,** 1986, 979.
13. Van Hove, L., *Phys. Rev.*, **89,** 1953, 1189.